Simulation-Assisted Efficient Computation of the Dispersion Diagram of Periodic Structures: A Comprehensive Overview With Applications to Filters, Leaky-Wave Antennas and Metasurfaces

Francisco Mesa, Guido Valerio, Raul Rodriguez-Berral, Oscar Quevedo-Teruel

Simulation-Assisted Efficient Computation of the Dispersion Diagram of Periodic Structures

Francisco Mesa, *Fellow, IEEE*, Guido Valerio, *Senior Member, IEEE*, Raúl Rodríguez-Berral, and Oscar Quevedo-Teruel, *Senior Member, IEEE*

***Abstract*—A hybrid method that combines the results of a commercial simulator with analytical post-processing is discussed and used to compute the dispersion diagrams of periodic structures. The method takes advantage of the ability of commercial simulators to deal with arbitrary geometries and materials and overcomes some of their limitations to compute the attenuation constant. The frequency behavior of the attenuation constant is very valuable for microwave and antenna design since it provides key information on the isolation/rejection in stopbands and the radiation losses in periodic leaky-wave antennas. A comprehensive overview of different theoretical and practical issues regarding the computation of dispersion diagrams is first carried out. Important considerations and main assumptions concerning the practical implementation of the method and its interaction with the commercial simulator are thoroughly discussed.**

***Index Terms*—Periodic structures, commercial simulators, dispersion diagram, radiation losses, leaky waves.**

I. Introduction

The knowledge of the dispersion diagrams of periodic structures is of capital relevance in the general study of wave propagation [1]–[3]. These diagrams provide insight on the behavior and interaction of the waves with the waveguiding environment: forward/backward and fast/slow wave nature, level of anisotropy and dispersion, existence and characteristics of band gaps, wave attenuation due to radiation or losses, etc. Assuming a time-harmonic dependence of the fields, the wave propagation in a one-dimensional (1-D) periodic structure along the direction of periodicity can mathematically be solved with a Floquet analysis. This means that the potentials/fields in the structure, denoted here in general as $\mathbf{C}$, satisfy the following condition [2]:

$$\mathbf{C}(x,y,z,t) = \mathbf{C}_p(x,y,z)\,\mathrm{e}^{-\gamma z}\,\mathrm{e}^{\mathrm{j}\omega t} \tag{1}$$

where ω is the angular frequency, $\gamma(\equiv \mathrm{j}k_z) = \alpha + \mathrm{j}\beta$ is the complex propagation constant along the assumed wave-propagation direction (z), with α being the attenuation constant and β the phase constant [$k_z = -\mathrm{j}\gamma = \beta - \mathrm{j}\alpha$ is the complex wavenumber along the z-direction]. The periodic function $\mathbf{C}_p$ satisfies $\mathbf{C}_p(x,y,z) = C_p(x,y,z+np)$, with np being an integer multiple of period of the structure. Starting from the general condition (1), the dispersion relations of periodic guiding/radiating electromagnetic structures have been computed with a large variety of methods. Following [4], these methods can be classified into two categories: (A) methods that compute the propagation constant at each frequency, and (B) methods that extract the frequency at which the unit cell of the periodic structure resonates when subject to a given phase shift along the periodicity direction.

One key issue that complicates any of the possible solution methods is the complex nature of the propagation constant (having both imaginary and real parts), which may occur for both bounded and unbounded waveguiding systems, even in the absence of material losses. However, there is an important difference between modal solutions of bounded and unbounded guiding structures. Bounded waveguiding systems, shielded by either electric/magnetic walls or periodic boundary conditions, always lead to wave equations that can be framed into the so-called Sturm-Liouville problems of the first kind [5]. Their modal analysis always yields eigenvalue problems with a discrete spectrum [2], [5], whose possible solutions are bound, evanescent, and complex modes [2], [6]–[8]. When other types of boundaries conditions and/or unbounded regions are present in the waveguiding system, the spectrum of the resulting eigenproblem has both continuous and discrete parts. As the continuous spectrum of any electromagnetic problem can be partly associated with the power radiated to the unbounded region [2], [5], complex leaky-wave modal solutions can now appear in the dispersion relation of the structure [2], [9], [10]. In general, the appearance of modes with complex propagation constants means that the solution of the modal characteristic equation requires extra mathematical and numerical tasks [2], [7], [10]. The scientific literature shows that a lot of effort has been devoted to find appropriate methods to search for the complex roots of the characteristic equations, or directly to avoid such root-searching.

Nowadays it is a very common practice the use of commercial full-wave simulators (HFSS, CST, FEKO, ADS,...) in the analysis and/or design of microwave and antenna devices. Certainly, the ability of these simulators to deal with very general structures is one of theirmost appreciated assets. The price to pay for this wide applicability is their often elevated demand of computational and memory resources. Concerning the calculation of dispersion diagrams, to the best of the authors' knowledge, existing simulators do not compute the complete dispersion diagram of all the modal solutions of periodic waveguiding systems but only the behavior of the phase shift (βp) vs. frequency and the attenuation constant due to material losses. However, the information of the attenuation

F. Mesa and R. Rodríguez-Berral are with Microwaves Group, Dept. of Applied Physics 1, ETS de Ingeniería Informática, Universidad de Sevilla, Spain (e-mail:mesa@us.es, rrberral@us.es).

G. Valerio is with Sorbonne Université, Laboratoire d Èlectronique et Électromagnétisme, UR2, L2E, F-75005 Paris, France (e-mail:guido.valerio@sorbonne-universite.fr).

O. Quevedo-Teruel is with the Division of Electromagnetic Engineering, KTH Royal Institute of Technology, 114 28 Stockholm, Sweden (e-mail: oscarqt@kth.se).

This work was partly supported by the Spanish Ministerio de Ciencia, Innovacion y Universidades and European Union FEDER funds under Project TEC2017-84724-P, the French National Research Agency Grant Number ANR-16-CE24-0030, the Vinnova project High-5 (2018-01522), under the Strategic Programme on Smart Electronic Systems, and the Stiftelsen forsk project H-Materials (18-302). The work of F. Mesa has also been funded by the Spanish Government (Salvador de Madariaga fellowship PRX19/00025). (Corresponding author: Oscar Quevedo-Teruel.)

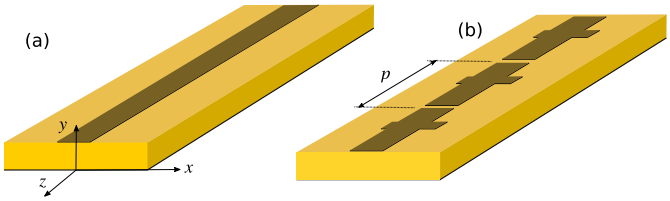

Fig. 1. Examples of (a) uniform waveguiding system, (b) one-dimensional periodic structure of period p.

constant is crucial for many lossless and radiating cases, specially in electromagnetic band gap structures as well as in leaky-wave antennas.

In this paper, we present a thorough discussion on how the so-called *multi-mode transfer-matrix method* [2], [4], [11]–[19] combines the simulator's advantage of dealing with a wide range of material and arbitrarily-shaped structures together with a convenient post-processing to compute the complete dispersion diagram of periodic structures. With this method one can obtain the information of the modal attenuation constant, regardless if they come either from losses, radiation, or the intrinsic complex/evanescent nature of the modes. Different novel aspects of the application of the method to unbounded radiative structures as well as two-dimensional (2-D) configurations are considered. Additionally, the presence of higher symmetries in the unit cell is also contemplated.

II. Analysis

In order to keep the discussion and analysis in this section as simple as possible, only 1-D periodicity will be considered. The extension to 2-D periodic structures will be treated later in Sec. III-B.

A. Eigenproblems in guided-wave analysis

Before discussing the periodic case, some of the main features of the uniform (non-periodic) problem in the frequency domain will be briefly outlined.

1) Uniform structures: In this situation, we have a structure invariant to arbitrary translations along the propagating z-direction as the one shown in Fig. 1(a). Regardless of the employed method of analysis, the procedure to find the modes of the structure [2], [20] will lead to an eigenproblem that can be expressed, in general, as

$$[\mathbf{\Gamma}(k_z,\omega)]\mathbf{u} = 0 \tag{2}$$

where k_z are the eigenvalues (modal wavenumbers) of the problem, $\mathbf{u}$ the corresponding eigenvectors, and $[\mathbf{\Gamma}]$ is the matrix associated with the projection method employed to solve the corresponding integral equation (IE); for instance, method of moments (MoM) [21], finite element method (FEM) [22], mode matching (MM) [23], Nystrom collocation method [24], etc. It should be noted that, in general, the above eigenproblem is non-linear and only under certain circumstances (for instance, the case of a homogeneous rectangular waveguide) it turns into a linear eigenproblem [25]. The BIRME method reported in [26] provides a procedure to linearize the eigenproblem for homogeneous waveguides with an arbitrary shape. Notwithstanding, the dispersion relation of the structure can always be expressed as the solution of

$$F(k_z;\omega) \equiv \det\{[\mathbf{\Gamma}(k_z,\omega)]\} = 0\,. \tag{3}$$

For each value of frequency ω, the solution of the above equation means searching for the complex zeros of the complex function $F(k_z)$. In general, this zero-searching is not simple, being one of the recurrent problems in the literature on modal analysis [27]–[31]. The two main reasons that make difficult to search numerically for complex zeros are: i) the function have poles and branch-point singularities, and ii) it is difficult to find a systematic and reliable algorithm that can explore the complex plane, which can comprise several Riemann sheets, without loosing any of the zeros of the function. Possibly because of these two underlying drawbacks, most commercial simulators avoid this zero-searching and do not usually provide the complete dispersion relation of uniform structures.

2) Periodic structures: If the modal analysis is to be applied to 1-D periodic structures (periodicity along the propagating z-direction) as the one shown in Fig. 1(b), the solution of the corresponding IE method also leads in general to a non-linear eigenvalue problem [32]. This means that the same difficulties involved in the obtaining of the dispersion relation of uniform structures also hold for 1-D periodic structures. Because of this, many efforts have been devoted to circumvent this problem and different alternatives have been reported in the literature to formulate an equivalent linear eigenproblem.

One possibility is to solve directly Maxwell's equations in the time domain. Examples of this procedure are the finite differences in the time domain (FDTD) methods reported, for example, in [33]–[36]. The approaches presented in [33], [34] could only deal with real propagation constants, but the possibility of losses/radiation was successfully incorporated in [35], [36]. Although these time-domain methods avoid the difficult task of searching for complex zeros, their intrinsic iterative nature involves very large, although sometimes sparse, matrices. This usually leads to intensive computational efforts and high demands of storage, apart from numerical instabilities that may appear when non-uniform grid meshing are required to deal with complex geometries as well as multi-scale structures. Similar problems can also be found in the finite difference in the frequency domain (FDFD) method reported in [4]. Enhanced implementations of FDTD and FDFD methods can partially alleviate some of the aforementioned problems, but this issue is beyond the scope of the present work, more focused on frequency-domain IE methods.

Another common approach to find the dispersion diagram as the solution of a linear eigemproblem is to model the 1-D periodic structure as a 2-port equivalent network characterized by its transfer (ABCD) matrix $[\mathbf{T}]$ and subject to periodic boundary conditions along the propagation direction [2], [25]. Next, two different implementation of this method will be briefly outlined before discussing a third method that can overcome most of the limitations of the previous two.

B. Method 1-uc: 2-port transfer matrix of a single unit cell

One of the most common and simple strategies consists in describing the periodic structure, which is invariant under

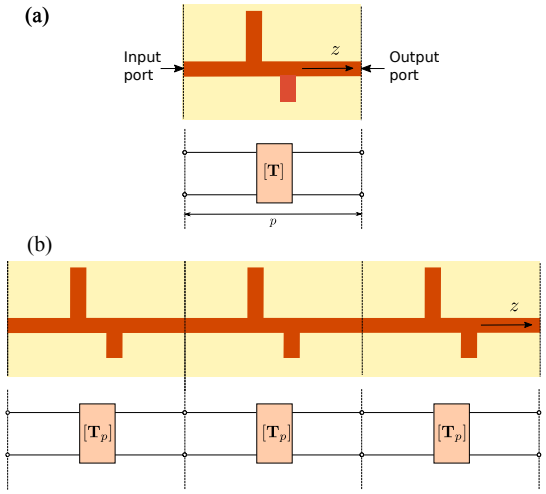

Fig. 2. (a) Top view of a single cell whose transfer matrix $[\mathbf{T}]$ is to be obtained. (b) Cascade of $[\mathbf{T}_p]$ matrices in the infinite structure. In method 1-uc it is assumed that $[\mathbf{T}_p] \approx [\mathbf{T}]$.

translations of an integer multiple of periods, as a *housing waveguide* loaded by some additional periodic elements (or *discontinuities*). The housing waveguide is uniform (i.e., invariant with respect to an arbitrary translation) and would support a certain number of modes in the absence of any periodic load. A transfer matrix $[\mathbf{T}]$ can then be associated with a single unit cell of the periodic structure, excited at its access ports by the fundamental mode of the housing waveguide, as shown in Fig. 2(a). For instance, in the unit cell shown in Fig. 1(b), the housing waveguide is a microstrip line and the "discontinuities" are the lateral metallic stubs placed on both sides of the conducting strip. Although such distinction between the housing waveguide and discontinuity is difficult in some structures, in principle, this decomposition can always be done. In this first simplified method, the original 1-D periodic electromagnetic problem can be modelled as a cascade of 2-port transfer matrices, as depicted in Fig. 2(b), where the actual transfer matrix, $[\mathbf{T}_p]$, of the unit cell within the periodic environment is assumed to be given by the transfer matrix $[\mathbf{T}]$ of the single unit cell taken isolated; i.e., $[\mathbf{T}_p] \approx [\mathbf{T}]$. Here it is worth pointing out the difference between the so-called $[\mathbf{T}]$ and $[\mathbf{T}_p]$ matrices. The $[\mathbf{T}]$ matrix corresponds to the transfer matrix of an isolated single unit cell, as shown in Fig. 2(a), whereas $[\mathbf{T}_p]$ matrix stands for the transfer matrix of the unit cell when this unit cell is part of the infinitely periodic structure. In principle, this last matrix cannot directly be obtained with a commercial simulator since the simulator can only deal with truncated finite structures having input/output ports.

Often, the discontinuities inside the unit cell can be well characterized by equivalent networks of reactive elements which are known in closed form [37], [38]. In this simplified situation, the transfer matrix of the single unit cell is easily computed from the transfer matrices that account for the fundamental-mode propagation in two housing-waveguide sections and the one corresponding to the discontinuity network. In more complex cases, the transfer matrix of the single unit cell at each frequency can be numerically obtained with the help of commercial simulators. Once the 2×2 transfer matrix $[\mathbf{T}]$ of the single unit cell

$$[\mathbf{T}] = \begin{bmatrix} A & B \\ C & D \end{bmatrix} \tag{4}$$

is obtained, the following eigenproblem is reached after applying a Floquet's analysis to solve for the complex propagation constant γ of the infinite periodic structure [2], [3], [25]:

$$[\mathbf{T}]\mathbf{u} = \mathrm{e}^{\gamma p}\mathbf{u}\ . \tag{5}$$

The $\mathbf{u}$ column matrix 2×1 is given by

$$\mathbf{u} = \begin{bmatrix} V \\ I \end{bmatrix} \tag{6}$$

with V and I being the voltage and current at the output port of the unit-cell problem. Under the assumption of reciprocity, the dispersion relation of the structure is then given by the following well-known expression [25, Eq. (8.7)]:

$$\cosh(\gamma p) = \frac{A(\omega) + D(\omega)}{2} \tag{7}$$

where the frequency dependence of the transfer-matrix entries is explicitly shown.

In the above simple procedure, at first sight, it may seem that the dispersion relation of the structure has been found eluding the zero-searching problem intrinsic to the non-linear eigenproblem associated with any general modal analysis. It should however be noted that the solution of the transfer matrix of a single unit cell via the 3-D full-wave commercial simulator has actually required a modal analysis of the input/output port; namely, the fundamental mode of the housing waveguide has been previously obtained. Only after this non-linear eigenproblem has been internally solved by the simulator, it is possible to compute the transfer matrix that leads to the linear eigenproblem in (5). A somewhat similar procedure is reported in [39] where a linear eigenvalue problem is solved after the corresponding integral equation. Other additional relevant issues and approximations implicit in the above procedure are [40]:

(i). Since only the fundamental mode of the housing waveguide is considered in the analysis, implicitly assumed through the approximation $[\mathbf{T}_p] \approx [\mathbf{T}]$, interactions between different unit cells supported by high-order modes of the housing waveguide are completely left out. This assumption is no longer valid when the electric size of the period is small as well as in many other practical situations that actually require to account for the high-order interactions between cells [2, Sec. 9.7].

(ii). If the housing waveguide is unbounded (for instance, a microstrip line without top cover), then only the discrete spectrum [2] of the housing waveguide is considered. This condition is intrinsically imposed by the commercial simulators when modelling the input and output ports as waveguiding systems that are bounded by either electric, magnetic, or periodic boundary conditions. As already mentioned, these boundary conditions always lead to discrete spectra. Thus, when the housing waveguide is unbounded, there is always an implicit detrimental approximation due to the different nature

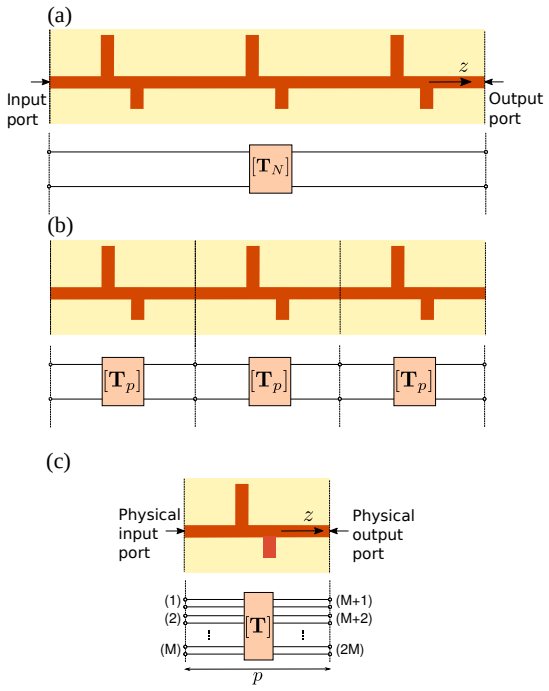

Fig. 3. (a) Top view of a N-cell structure whose transfer matrix $[\mathbf{T}_N]$ is to be obtained. (b) Cascade of $[\mathbf{T}_p]$ matrices in the infinite structure. In method N-uc it is assumed that $[\mathbf{T}_p] \approx \sqrt[N]{[\mathbf{T}_N]}$. (c) Finite structure with a single unit cell whose high-order mode transfer matrix $[\mathbf{T}]$ is to be obtained.

of the spectrum of the input/output ports and the one of the housing waveguide, occasionally enhanced by their possible mismatches. Although this drawback may be hardly relevant in many practical circumstances when dealing with *bounded* fields in open structures, the appropriate characterization of the reflected/transmitted power when radiation is present would require a more careful choice of the input/output ports. In these circumstances, one possible solution could be to ensure that additional variations in the height of the ports do not affect the results of the scattering parameters. More discussions about this issue will be further conducted when the numerical examples are discussed in Sec. IV.

C. Method N-uc: 2-port transfer matrix of N unit cells

In principle, to the authors' knowledge, not much can be done to circumvent the drawback (ii) when significant, although possible alternatives, involving the development of the in-house full-wave eigenmode solver, have been proposed in [41], [42]. However, different solutions involving commercial simulators have been reported to overcome the drawback (i) [43]–[46]. A common procedure, graphically sketched in Figs. 3(a) and (b), is to consider a finite system of multiple unit cells, say N, and assume that the 2-port transfer matrix of this N-cell system, $[\mathbf{T}_N]$, is related to the transfer matrix of the unit cell in the periodic environment as follows [47]:

$$[\mathbf{T}_p] = \sqrt[N]{[\mathbf{T}_N]}\ . \tag{8}$$

The drawbacks (i) and (ii) are still present at the two ports of the N-cell system. Nevertheless, they are partially mitigated with the computation of the coupling between the unit cells inside the system, since the inner boundaries between cells are no more described by equivalent bounded and monomodal ports. It is this fact what is expected to increase the precision of the mutual interactions among cells as N increases. Still, numerical problems also affect this procedure [47]. Among them it can be mentioned the eventual high computational cost of having to analyze a finite structure with many cells, which can easily lead to numerical noise and inaccuracies. Another relevant problem comes from the inherent ambiguity in the propagation-constant solutions of the N-cell problem because of the non-uniqueness of the Nth root of a complex number. This leads to an ambiguity on the value of the phase constant which needs to be addressed; e.g., as in [47]. Furthermore, the case of a LWA that required many unit cells to characterize accurately its complex propagation constant but with a non-small radiation attenuation could pose an important numerical problem due to the almost negligible values of the field at the output port of the N-cell structure.

III. Proposed Methodology

A methodology that can overcome most of the aforementioned drawbacks will be discussed in this section. First, it should be reminded that the main limitation of the frequency-domain eigenmode solver of commercial simulators comes from the difficulties to provide the complex modal attenuation constants of periodic structures, regardless if losses come from either the evanescent/complex nature of the modes or the presence of unbounded/lossy regions in the periodic structure. Nevertheless it is apparent that commercial simulators can deal efficiently with unbounded/lossy structures with regards to the computation of the scattering parameters of such structure.

A. 1-D Periodic Structures

For the simpler case of 1-D periodic structures, the corresponding transfer matrix of an isolated unit cell can easily be obtained from the scattering matrix of the structure modeled as a 2-port network [25]. However, as previously discussed in Sec. II-A2, the use of two-port transfer matrix also brings some drawbacks. Hence, in similarity to [2], [4], [11]–[18], it is proposed to keep on using the transfer matrix of a *single* unit cell of the periodic structure but extend its capabilities by modeling this unit cell as a *multiport* transfer matrix that takes into account multiple modes of the structure. A graphical representation of this procedure is shown in Fig. 3(c). In doing so, the inter-cell coupling effect due to high-order modes can now be well accounted for, an effect that method 1-uc in Sec. II-B could not take into account. Very often the use of multiport equivalent networks is associated with the actual presence of more than two physical ports (terminals) in the structure [15], [48]. However, it is well known that this requirement is not necessary, and the ports can equally be associated with the different modes (propagative, evanescent,...) of a structure with just one input and one output physical terminals [2], [3], [37].

For a multiport (or multi-mode) system, the transformation from the scattering matrix [49], [50] to the transfer matrix [51] is not direct but it can easily be carried out once the input and output ports of the structure are clearly defined. For this purpose, let us consider a balanced $2M$-port system whose input ports are numbered $1, 2, \ldots, M$, corresponding to the

first M significant modes, and output ports $M+1,\ldots,2M$ [see Fig. 3(c)] associated with the same set of significant modes. In order to find the multiport (multi-mode) transfer matrix, the scattering matrix is written in terms of four partitioned submatrices as

$$[\mathbf{S}] = \begin{bmatrix} [\mathbf{S}_{ii}] & [\mathbf{S}_{io}] \\ [\mathbf{S}_{oi}] & [\mathbf{S}_{oo}] \end{bmatrix} \tag{9}$$

where subscripts i and o stand for input and output ports, respectively, and each submatrix corresponds to the generalized scattering matrix that relates the input/output M modes. The multiport (multi-mode) transfer matrix can be obtained following, for instance, the derivations reported in [51], [52]. Alternatively, some relatively simple algebra operations lead us to the following expressions for the block-matrix elements of the transfer matrix:

$$[\mathbf{T}] = \begin{bmatrix} [\mathbf{A}] & [\mathbf{B}] \\ [\mathbf{C}] & [\mathbf{D}] \end{bmatrix} \tag{10}$$

where

$$[\mathbf{A}] = \frac{1}{2}\left[([\mathbf{1}]+[\mathbf{S}_{ii}])[\mathbf{S}_{oi}]^{-1}([\mathbf{1}]-[\mathbf{S}_{oo}])+[\mathbf{S}_{io}]\right] \tag{11}$$

$$[\mathbf{B}] = \frac{1}{2}\left[([\mathbf{1}]+[\mathbf{S}_{ii}])[\mathbf{S}_{oi}]^{-1}([\mathbf{1}]+[\mathbf{S}_{oo}])-[\mathbf{S}_{io}]\right][\mathbf{Z}_o] \tag{12}$$

$$[\mathbf{C}] = \frac{1}{2}[\mathbf{Z}_i]^{-1}\left[([\mathbf{1}]-[\mathbf{S}_{ii}])[\mathbf{S}_{oi}]^{-1}([\mathbf{1}]-[\mathbf{S}_{oo}])-[\mathbf{S}_{io}]\right] \tag{13}$$

$$[\mathbf{D}] = \frac{1}{2}[\mathbf{Z}_i]^{-1}\left[([\mathbf{1}]-[\mathbf{S}_{ii}])[\mathbf{S}_{oi}]^{-1}([\mathbf{1}]+[\mathbf{S}_{oo}])+[\mathbf{S}_{io}]\right][\mathbf{Z}_o] \tag{14}$$

with $[\mathbf{1}]$ being the $M\times M$ unit matrix and $[\mathbf{Z}_i]$ and $[\mathbf{Z}_o]$ square matrices whose diagonal elements are the input/output characteristic port impedances; namely

$$[\mathbf{Z}_{i/o}] = [\mathrm{diag}(Z_{i/o,m})]\ . \tag{15}$$

An interesting question that arises here is that the specific values of the impedances of the ports do not have any effect on the eigenvalues of the multiport transfer matrix as long as the same value is employed for the same mode at the input and output ports (that is, if $[\mathbf{Z}_i]=[\mathbf{Z}_o]$). This can easily be seen by rewriting the $[\mathbf{T}]$ matrix as

$$[\mathbf{T}] = \begin{bmatrix} [\mathbf{1}] & [\mathbf{0}] \\ [\mathbf{0}] & [\mathbf{Z}_i]^{-1} \end{bmatrix}[\mathbf{T}_1]\begin{bmatrix} [\mathbf{1}] & [\mathbf{0}] \\ [\mathbf{0}] & [\mathbf{Z}_o] \end{bmatrix} \tag{16}$$

where $[\mathbf{T}_1]$ stands for the transfer matrix defined with unitary port impedances and $[\mathbf{0}]$ for the $M\times M$ null matrix. As long as $[\mathbf{Z}_i]=[\mathbf{Z}_o]$, $[\mathbf{T}]$ is similar to $[\mathbf{T}_1]$ for any choice of the port impedances, and its eigenvalues are then invariant under a change of the impedances.

Assuming now that the above multi-mode $[\mathbf{T}]$ matrix is a good approximation of the multi-mode transfer matrix of the unit cell in the periodic environment, the eigenproblem to be solved is [2], [11], [12], [15]–[19]

$$[\mathbf{T}]\begin{bmatrix}\mathbf{V}\\ \mathbf{I}\end{bmatrix} = \mathrm{e}^{\gamma p}\begin{bmatrix}\mathbf{V}\\ \mathbf{I}\end{bmatrix} \tag{17}$$

where $\mathbf{V}$ and $\mathbf{I}$ are now $M\times 1$ arrays containing the voltages and currents at the output ports. This eigenproblem is formally identical to (5) for the two-port case. The only relevant difference is that we will find M pairs of eigenvalues associated with $\pm\gamma_m p$ ($m=1,\ldots,M$).

If the unit cell under study is reciprocal, the inverse of the transfer matrix satisfies [51, Eq. (51)]

$$[\mathbf{T}]^{-1} = \begin{bmatrix} [\mathbf{D}]^T & -[\mathbf{B}]^T \\ -[\mathbf{C}]^T & [\mathbf{A}]^T \end{bmatrix} \tag{18}$$

where superscript T means transpose. For this matrix the following eigenvalue problem holds:

$$[\mathbf{T}]^{-1}\begin{bmatrix}\mathbf{V}\\ \mathbf{I}\end{bmatrix} = \mathrm{e}^{-\gamma p}\begin{bmatrix}\mathbf{V}\\ \mathbf{I}\end{bmatrix}\ . \tag{19}$$

Summing the eigenproblems (17) and (19) for the multi-mode transfer and inverse-transfer matrices, the following eigenvalue problem is obtained:

$$\begin{bmatrix} [\mathbf{A}]+[\mathbf{D}]^T & [\mathbf{B}]-[\mathbf{B}]^T \\ [\mathbf{C}]-[\mathbf{C}]^T & [\mathbf{D}]+[\mathbf{A}]^T \end{bmatrix}\begin{bmatrix}\mathbf{V}\\ \mathbf{I}\end{bmatrix} = 2\cosh(\gamma p)\begin{bmatrix}\mathbf{V}\\ \mathbf{I}\end{bmatrix} \tag{20}$$

which turns out to have two degenerate set of eigenvalues; namely, each $\gamma_m p$ is a double solution of (20). If the structure is also symmetric, then $[\mathbf{A}]=[\mathbf{D}]^T$, $[\mathbf{B}]=[\mathbf{B}]^T$, and $[\mathbf{C}]=[\mathbf{C}]^T$ [51]. This means that the above $2M$-rank eigenproblem can be reduced to the M-rank one given by

$$[\mathbf{A}]\mathbf{V} = \cosh(\gamma p)\mathbf{V}\ . \tag{21}$$

The above eigenproblem clearly simplifies to the well-know dispersion relation provided in (7) for the simplest case of a 2-port symmetric periodic structure.

An interesting practical situation arises if the unit cell under study has any kind of internal higher symmetry (for instance, glide [53] or twist [54] symmetries). In this case, the eigenvalue problem can be set up for the so-called sub-unit cell (the size of which will be denoted as $\hat{p}$) where the corresponding higher symmetry operator plays the same role as the Floquet translation-symmetry operator for a standard periodic structure [19], [39], [53], [55]. The resulting generalized eigenvalue problem can then be written, following the notation in [19], [55], as

$$[\hat{\mathbf{T}}]\begin{bmatrix}\mathbf{V}\\ \mathbf{I}\end{bmatrix} = \mathrm{e}^{\gamma\hat{p}}\begin{bmatrix} [\mathbf{Q}] & [\mathbf{0}] \\ [\mathbf{0}] & [\mathbf{Q}] \end{bmatrix}\begin{bmatrix}\mathbf{V}\\ \mathbf{I}\end{bmatrix} \tag{22}$$

where $[\hat{\mathbf{T}}]$ is the corresponding multi-mode transfer matrix for the sub-unit cell and $[\mathbf{Q}]$ is a submatrix that accounts for the corresponding algebraic operations resulting from the effects of the specific higher symmetry on the electric/magnetic fields; more details can be found in the Appendix and in [19], [55]. Dealing directly with the eigenvalue problem in (22) leads to numerical and accuracy advantages since it reduces considerably the size of the structure to be analyzed with the full-wave simulator. If the system is reciprocal and symmetric, the eigenvalue problem can be further simplified [in analogy with (21)] into

$$[\hat{\mathbf{A}}]\mathbf{V} = \frac{1}{2}\left\{\mathrm{e}^{\gamma\hat{p}}[\mathbf{Q}]+\mathrm{e}^{-\gamma\hat{p}}[\mathbf{Q}]^{-1}\right\}\mathbf{V}\ . \tag{23}$$

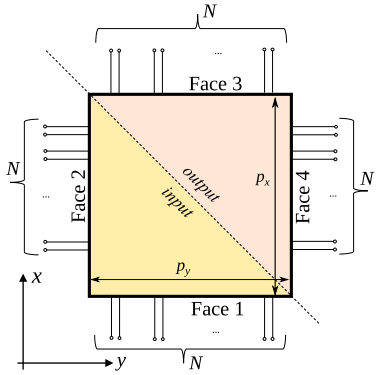

Fig. 4. Top view of a unit cell of a 2-D periodic structure, with periodicity along the x and y directions. N modes are retained on each of the four geometrical faces.

B. 2-D Periodic Structures

The multi-mode transfer-matrix method can straightforwardly be used for the study of 2-D periodic structures [19]. With reference to Fig. 4, the unit cell of this problem can be described as a region accessible through four geometrical faces, numbered from 1 to 4. Faces 1 and 2 are here considered as *input* faces, and 3 and 4 as *output* faces. On each face, M modes can be defined as done in the previous section. Each mode of each face is then associated with a port. In this way, the cell is associated with a $4M$-port network. A commercial software can easily extract the scattering matrix of this network as in (9), where each sub-matrix has now dimensions $2M \times 2M$. More specifically, the 2-D version of the submatrices in (9) can be written in the following block form where the couplings among the four different geometrical faces appear explicitly:

$$[\mathbf{S}_{ii}] = \begin{bmatrix} [\mathbf{S}_{11}] & [\mathbf{S}_{12}] \\ [\mathbf{S}_{21}] & [\mathbf{S}_{22}] \end{bmatrix} \qquad [\mathbf{S}_{io}] = \begin{bmatrix} [\mathbf{S}_{13}] & [\mathbf{S}_{14}] \\ [\mathbf{S}_{23}] & [\mathbf{S}_{24}] \end{bmatrix}$$

$$[\mathbf{S}_{oi}] = \begin{bmatrix} [\mathbf{S}_{31}] & [\mathbf{S}_{32}] \\ [\mathbf{S}_{41}] & [\mathbf{S}_{42}] \end{bmatrix} \qquad [\mathbf{S}_{oo}] = \begin{bmatrix} [\mathbf{S}_{33}] & [\mathbf{S}_{34}] \\ [\mathbf{S}_{43}] & [\mathbf{S}_{44}] \end{bmatrix} . \tag{24}$$

The transfer matrix can then be computed by using the same equations (11)–(14). This matrix operates a transformation from the output to the input ports as

$$\begin{bmatrix} \mathbf{V}_1 \\ \mathbf{V}_2 \\ \mathbf{I}_1 \\ \mathbf{I}_2 \end{bmatrix} = [\mathbf{T}] \begin{bmatrix} \mathbf{V}_3 \\ \mathbf{V}_4 \\ \mathbf{I}_3 \\ \mathbf{I}_4 \end{bmatrix} . \tag{25}$$

In 2-D periodic structures, Floquet boundary conditions should be enforced along the two periodicity axes as $\mathbf{V}_3 = \mathrm{e}^{-\gamma_x p_x}\mathbf{V}_1$ and $\mathbf{V}_4 = \mathrm{e}^{-\gamma_y p_y}\mathbf{V}_2$, and equivalently for the currents (being p_x and p_y the periods along x and y directions). From (25), these conditions can be formulated as the following eigenvalue problem:

$$[\mathbf{T}] \begin{bmatrix} \mathbf{V}_3 \\ \mathbf{V}_4 \\ \mathbf{I}_3 \\ \mathbf{I}_4 \end{bmatrix} = \begin{bmatrix} \mathrm{e}^{\gamma_x p_x}\mathbf{V}_3 \\ \mathrm{e}^{\gamma_y p_y}\mathbf{V}_4 \\ \mathrm{e}^{\gamma_x p_x}\mathbf{I}_3 \\ \mathrm{e}^{\gamma_y p_y}\mathbf{I}_4 \end{bmatrix} = [\mathbf{B}(\gamma_x p_x, \gamma_y p_y)] \begin{bmatrix} \mathbf{V}_3 \\ \mathbf{V}_4 \\ \mathbf{I}_3 \\ \mathbf{I}_4 \end{bmatrix} \tag{26}$$

where

$$[\mathbf{B}] = \begin{bmatrix} \mathrm{e}^{\gamma_x p_x}[\mathbf{1}] & [\mathbf{0}] & [\mathbf{0}] & [\mathbf{0}] \\ [\mathbf{0}] & \mathrm{e}^{\gamma_y p_y}[\mathbf{1}] & [\mathbf{0}] & [\mathbf{0}] \\ [\mathbf{0}] & [\mathbf{0}] & \mathrm{e}^{\gamma_x p_x}[\mathbf{1}] & [\mathbf{0}] \\ [\mathbf{0}] & [\mathbf{0}] & [\mathbf{0}] & \mathrm{e}^{\gamma_y p_y}[\mathbf{1}] \end{bmatrix} . \tag{27}$$

Unlike the eigenproblem (17), the one in (26) is not linear and, in general, is expected to be solved numerically for the unknown complex phase shifts $\gamma_x p_x$ and $\gamma_y p_y$. The right-hand side of (26) is brought to the left thus obtaining an eigenvalue problem of the kind given in (2). The phase shifts can then be computed in general as the solution of

$$\det\{[\mathbf{T}(\omega)] - [\mathbf{B}(\gamma_x p_x, \gamma_y p_y)]\} = 0 \tag{28}$$

by means of an appropriate zero-searching algorithm. Fortunately, the transfer matrix $[\mathbf{T}(\omega)]$, which is the only part of (28) requiring the solution of a full-wave problem, has only to be obtained once at each frequency in this zero-searching process, which simplifies considerably the numerical procedure. In most cases, only few cuts of the Brillouin diagram are required. For example, an irreducible zone of a unit cell symmetric with respect to its center (namely, $p_x = p_y$) should be plotted along three spectral directions: (i) $\gamma_y = 0$, the problem (26) is solved for $\gamma_x p_x$; (ii) $\gamma_x p_x = \mathrm{j}\pi$, the problem (26) is solved for $\gamma_y p_y$; and (iii) $\gamma_x = \gamma_y$, the problem (26) is solved for $\gamma_x p_x = \gamma_y p_y$. Although in these three cases, there is only one unknown, only the latter case (iii) leads to a standard linear eigenvalue problem.

Finally, it is interesting to remark that the multi-cell method [43]–[47], here denoted as method N-uc, cannot directly be extended to obtain the complete dispersion diagram of 2-D periodic structures, since at least four ports are required to define the access to the unit cell (or, equivalently, to the N-cell system) and a 2×2 transfer matrix cannot describe all possible propagation directions in this case. Actually, only the conditions of propagation along the principal axes of the structure could be satisfactorily implemented with the multi-cell method. This means that the propagation along x- and y-directions (having $k_y = 0$ and $k_x = 0$, respectively) can be implemented with a chain of N 2-D unit cells along the the same direction and periodic boundary conditions in the 2-D unit cells at $y = 0$ or $x = 0$ and $y = P_y$ or $x = P_x$. However, propagation under any other condition (including $k_x = k_y$) is quite difficult to reproduce by a 1-D chain of 2-D unit cells. Also, it should be noted that the present multi-modal method could be used in a similar way for the study of 3-D periodic structures, although this case is beyond the scope of this paper.

IV. Results

The multi-mode transfer-matrix method discussed in previous section will be denoted in this section as "HOm" method (from high-order modes). This proposed methodology will be validated with a number of examples, including some novel periodic structures. Through these examples, we will discuss some important practical issues to be taken into account in the implementation of the method. One of the most important practical consideration found by the authors concerning the suitable application of the method is that, when computing the

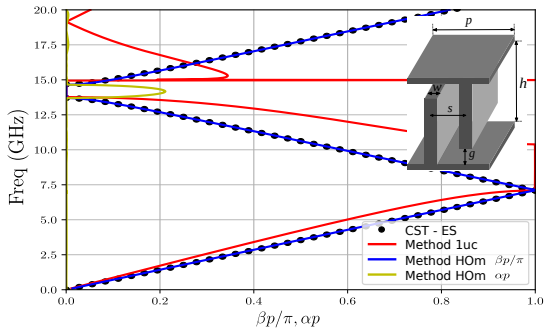

Fig. 5. Dispersion diagram of a parallel-plate waveguide with corrugations having glide symmetry. Results from Method HOm are computed with $M = 3$ modes. The inset of the figure shows a cross view of the unit cell with dimensions: $p = 6$ mm, $h = 10$ mm, $s = 2$ mm, $w = 1$ mm, and $g = 1$ mm.

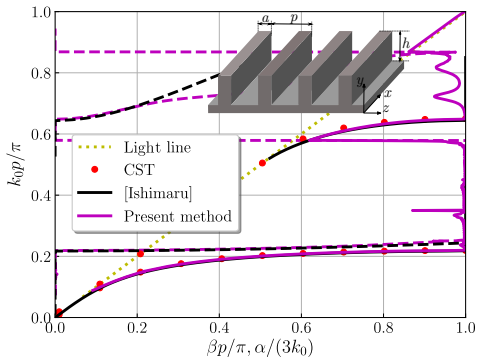

Fig. 6. Dispersion diagram ($\beta p/\pi$: solid lines, $\alpha/(3k_0)$: dashed lines) of a 1-D corrugated perfect-conductor surface. Dimensions: $a = 0.8p$, $h = 2p$. Our HOm data ($M = 5$) are compared with CST and [6, Eq. (7-22)]

generalized scattering matrix with the full-wave EM simulator, the input/output ports should be located at planes of the unit cell whose domain of definition ensures that the combination of the multiple modes at the input/output waveguide ports can account appropriately for the spatial variations caused by the discontinuities in these ports. This "general rule" for the location of the ports will lead to different port choices in the specific application cases to be next discussed. Another important consideration concerns the number and type of modes to be set in the ports. Again, every specific structure under study will demand a previous analysis of the situation, although following again the previous "general rule", the choice of modes should be guided by the required spatial variations imposed by the discontinuities inside the unit cell. For instance, strong spatial variation along one of the transverse dimensions of the unit cell would be a hint that some high-order modes associated to this spatial direction would be required. The above considerations have been applied in the following study cases, with the number of modes finally employed in each case being dictated by the good convergence of the values of the phase and attenuation constants.

The first validation example is the corrugated parallel-plate waveguide already studied in [40, Fig. 6]. In that work, it was shown that, when the corrugations have glide symmetry and are electrically close, the method 1-uc did not work well and method N-uc required at least five cells ($N = 5$) to match the CST results. If the present HOm method is now applied to a single unit cell of the structure, it can be checked in Fig. 5 that the phase shift ($\beta p/\pi$) given by this method is in very good agreement with CST results when three modes are employed. The HOm method also provides the values of the attenuation constant (αp), which can be seen to be only different from zero in the stop-band between 13.7 and 14.7 GHz. The obtaining of the attenuation constant in the stop-band can be very relevant from a practical point of view because small values of αp would lead to non-negligible levels of transmission in finite periodic structures. Thus, for practical finite periodic structures (made up of N unit cells), the stop-band should be defined as that frequency band where αNp is beyond certain threshold; for instance, $\alpha Np = \ln 10$ to ensure $|S_{21}| < -20$ dB. For computing the generalized scattering matrix with the commercial simulator, the unit-cell geometry has been taken as shown in the inset of Fig. 5. If the unit cell were defined with input/output ports at the center of the metal corrugations, the performance of the HOm method would be rather poor since the high-order modes at the ports would be hardly congruent with the vertical variations caused by the corrugations in these ports. Also, since the present 1-D case has no spatial variation along the transverse direction, the transverse electrical size of the unit cell has been taken small and bounded by perfect magnetic walls. These last conditions will ensure that the modes in the ports would resemble the modes of a parallel-plate waveguide.

The next structure to be analyzed is the 1-D metal corrugated surface [6] shown in the inset of Fig. 6. The phase shift of this structure computed by HOm is found to be in good agreement with the values provided by CST as well as with the approximated formula in [6, Eq. (7-22)]. The attenuation constant provided by the HOm method shows a partial agreement with the results provided by [6, Eq. (7-22)], fact that is somewhat expected due to the approximate nature of this expression (values of $\alpha/(3k_0)$ are plotted in Fig. 6 in order to fit the range of variation of the attenuation constant). The HOm results are found to converge when five modes ($M = 5$) are used in the method, fact that can be considered as a test of self-consistency of the method. The CST values of the generalized scattering matrix for this structure were obtained with waveguide ports located in the groove of the corrugations. In our experience, and in similarity with the structure above, the input/output ports should be located inside the groove, rather than in the middle of the corrugations. In the present open-boundary situation, the ports have to be few times larger than the corrugations to correctly model the attenuation constant. For this specific case, we have considered a port which is four times the height of the corrugations.

A third example, shown in Fig. 7, is a LWA already treated in [56] consisting in a microstrip line periodically loaded with vertical central vias. In this kind of leaky-wave structures, the obtaining of the dispersion diagram for the attenuation constant is key for design purposes and, therefore, robust methods for its computation are of high practical relevance. The results of the HOm method are found to agree well with those provided by the IE method reported in [32] and the multiple-cell approach discussed in [56]. Only three high-order modes are necessary to obtain a good convergence in the HOm method in this structure. It should be noted that the

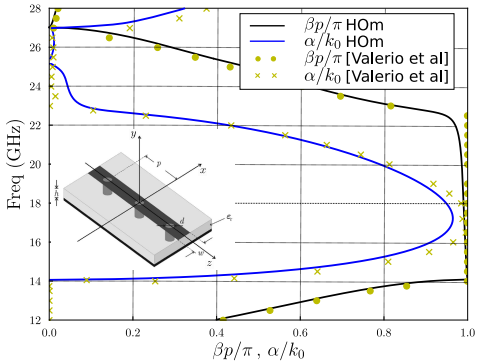

Fig. 7. Dispersion diagram of a microstrip leaky-wave antenna with vertical vias, already studied in [56, Fig. 10]. HOm results have been obtained with three modes ($M = 3$).

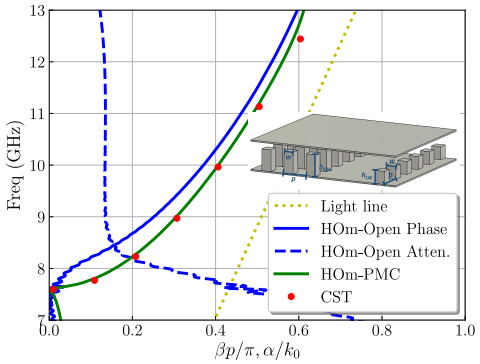

Fig. 8. Dispersion diagram of a groove-gap waveguide studied in [57, Fig. 2]. The groove waveguide corresponds to the standard WR-90. The dimensions are: w = 3 mm, p = 8.5 mm, h_{LW} = 3.5 mm, h_{EBG} = 7.5 mm.

method accounts well for the proper and improper leaky-wave solutions shown in Fig. 7; more details about these solutions are discussed in [32].

A final 1-D structure to be analyzed is the groove-gap waveguide structure shown in the inset of Fig. 8. This waveguide was used as the underlying leakage system for the high-performance LWA reported in [58]. The structure is composed of a central waveguide region laterally bounded on the left by three rows of EBG pins and on the right by one row of "leaky-wave" pins that allow for radiation. Top and bottom PEC plates shield the waveguide in the vertical direction. A preliminary study of the dispersion diagrams of the partial waveguides that make up this complete waveguide was shown in [57, Fig. 2]. Now, the complete waveguide unit cell is analyzed by means of the HOm method both in the case of transverse perfect matching layers (PML), *open* in CST, and perfect magnetic conductors (PMC) boundary conditions. Only the results of this latter case are compared with the dispersion diagram computed using CST since the eigenmode solver of CST can only deal with shielded scenarios, as previously discussed in Sec. II-A2. The agreement for the phase shift of CST results with the HOm-PMC ones is very good but these results are slightly different to the HOm-Open ones corresponding to the more realistic waveguide with open lateral conditions that now allows for radiation (key in this LWA structure). The attenuation constant of the leaky-wave waveguide is also shown in the figure and its values are found to converge when

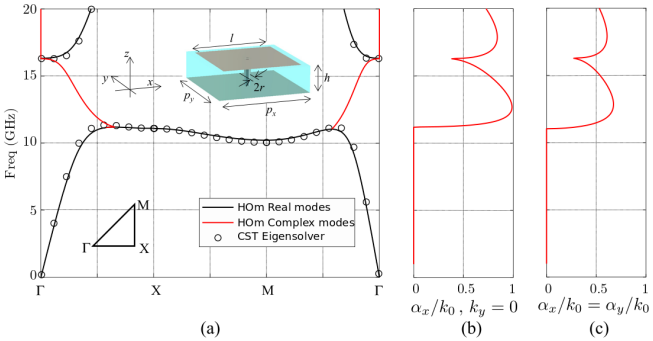

Fig. 9. 2-D dispersion diagram of the mushroom metasurface shown in the inset. $h = 1$ mm, $p_x = p_y = 3.5$ mm, $l = 3$ mm, $2r = 0.5$ mm, substrate with $\varepsilon_r = 2.2$. (a) Phase constant $\beta p/\pi$ in the irreducible Brillouin zone. Normalized attenuation constant α_x/k_0 with (b) $k_y = 0$ and (c) $k_y = k_x$.

five modes ($M = 5$) are employed in the HOm method. The scattering parameters were obtained with the time-domain solver of CST, with waveguide ports defined at the center of the pins. In this manner, CST provides the three first modes as those which can propagate through the EBG pins below the EBG frequencies, a fourth mode that mainly propagates in the "leaky-wave" pin, and a fifth mode which mainly propagates in the groove waveguide. The latter is the mode in which we are mainly interested in this specific design. PML (*open* condition in CST) was defined at the right side of the "leaky-wave" pin to emulate a perfect radiation without reflections.

In order to confirm the versatility of the HOm approach when applied to 2-D periodic structures as described in Section III-B, two further 2-D periodic structures are analyzed next. Figure 9 shows the full dispersion diagram of the 2-D periodic mushroom surface in the inset. The structure was simulated with a metallic plate on the top; since the results concern bound modes, the diagram is not affected by the presence of this top plate, as verified by varying its distance from the surface. The segment Γ-X shows the phase constant in the interval $0 \leq \beta_x p_x \leq \pi$ and $k_y = 0$; the segment X-M shows the phase constant in the interval $0 \leq \beta_y p_y \leq \pi$ and $k_x p_x = \pi$; the segment M-Γ shows the phase constant in the interval $\pi \geq \beta_x p_x \geq 0$ and $k_x = k_y$. The phase shifts obtained with the HOm method (solid curves) are validated with the results from the CST eigenmode solver simulations (circles) when related to real modes, with a perfect agreement found in the entire frequency range considered. The attenuation constants of complex modes, normalized to the free-space wavenumber, are shown in separate subfigures for each propagation direction. In the HOm analysis, $M = 9$ modes have been employed on each one of the fours geometrical faces defined on the boundary of the unit cell to ensure convergence of the results shown here.

Concerning the Γ-X section of the diagram in Fig. 9, only bound real modes propagate up to 11.2 GHz along the x direction of the surface (black line). At 11.2 GHz, two real modes merge into two complex conjugate modes (only one is shown in the picture, in red line). The phase constant of the complex mode varies until 16.35 GHz, and then it becomes zero at higher frequencies, but its attenuation constant stays

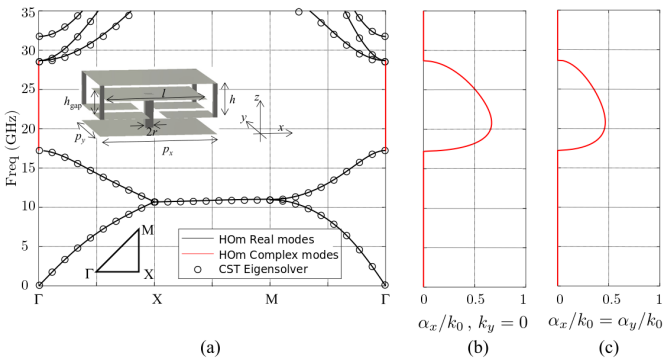

Fig. 10. 2-D dispersion diagram of the glide-symmetric mushroom metasurface shown in the inset. $h = 1\,\text{mm}$, $h_{\text{gap}} = 0.5\,\text{mm}$, $p_x = p_y = 3.5\,\text{mm}$, $l = 3\,\text{mm}$, $2r = 0.5\,\text{mm}$. No dielectric substrate is used. (a) Phase shift, $\beta p/\pi$, in the irreducible Brillouin zone. Normalized attenuation constant α_x/k_0 with (b) $k_y = 0$ and (c) $k_y = k_x$.

different from zero. These complex modes are not validated with CST since they cannot be recovered by the eigenmode solver tool. At 11.35 GHz another higher-order real mode starts propagating along the x direction. The X-M section of the diagram shows that when the propagation is studied along the y direction with $k_x p_x = \pi$, only one real mode propagates between 10.05 GHz and 11.1 GHz. Finally, the M-Γ section of the diagram shows the propagation along the diagonal of the unit cell, where $k_x = k_y$, and a similar behaviour as the one along the x direction is observed, with a stop-band from 11.08 GHz to 16.47 GHz, where a complex mode is shown in red together with its attenuation constant.

The same analysis as before is performed in Fig. 10 with two mushroom surfaces placed in a glide-symmetric configuration; i.e., mirrored with respect to a plane parallel to the surface and off-shifted half a period in both periodicity directions. Although 1-D glide symmetry was first studied in the 60's and 70's [53], new applications have recently found for 2-D glide-symmetric periodic structures [59], [60]. As explained in [19], glide symmetry can strongly modify the dispersion properties of 2-D periodic structures. The results in Fig. 10 are again simulated with nine modes on each geometrical face and plotted in a 2-D Brillouin diagram. As usual, the glide symmetry suppressed the stop-band at the X point present in the previous non-glide case. Now a real mode is present up to 17.22 GHz, and a stop-band arises this time at the Γ point between 17.22 GHz and 28.52 GHz, where a complex mode has been found with the HOm method (and again, not validated with the CST eigenmode solver tool since complex modes cannot be recovered with it). At 28.52 GHz two real modes start propagating and at 31.72 GHz another higher-order real mode starts propagating. These modes are recovered also with the CST eigenmode solver. In the X-M propagation direction, one propagating mode is found. This mode has a double multiplicity since it can be regarded as the merging of the two real branches reaching X coming from Γ. In the M-Γ section a similar behaviour as the one along the x direction is observed with the absence of a stop-band at the M point, a complex mode responsible of a stop-band between 17.4 GHz and 28.4 GHz, and three higher-order modes that start propagating at 28.64 GHz (two of them) and at 31.72 GHz.

V. Conclusions

Here we have described and discussed on an efficient method to calculate the dispersion diagram of periodic structures by using scattering simulations of a single unit cell. More specifically, the diagram is obtained after post-processing the scattering matrices computed with commercial software for an isolated single unit cell that is fed with two/four ports, which in turn are excited with multiple modes.

The main advantage of the method is that it can calculate both phase and attenuation constants. In particular, the attenuation constant due to leaky-modes and stop-bands cannot be calculated with the eigenmode solver of commercial software. In fact, the only possible computational methods for the leaky-wave attenuation are *i)* rigorous source-free full-wave time- or frequency-domain solvers enforcing complex Floquet-conditions at the periodic boundaries, or *ii)* scattering simulations of multiple unit cells excited with one single mode, leading to much longer computation time and possibly to loss of accuracy if the macro-cell becomes very large.

The proposed method enables a fast, accurate and comprehensive calculation of this attenuation constant. We validated the method with 1-D/2-D, bounded/unbounded, and conventional/glide-symmetric periodic structures. We also provided some guidelines to overcome the possible errors and limitations of applying this method. In particular, we identified that the location, number and type of the modes when computing the scattering parameters in the commercial software is critical. In our experience, some of the the most relevant practical aspects to be considered are the following:

- The position of the input/output ports has been chosen so that the unit cell is as symmetric as possible. In our experience, the most convenient choice is to locate the ports at the housing waveguide.
- In case of open structures, the height of the ports should be larger than the material structure to account for the possible radiation leakage emanating from the structure. However, this height should not be too large in order to avoid the presence of higher modes related to the ports which do not have any relevant role in the field behavior of the unit cell.
- The number and type of modes to be chosen in the waveguide ports should be selected taking into account the geometrical configuration of the discontinuity inside the unit cell so that the spatial variations caused by this discontinuity at the waveguide ports locations can be well matched with the set of modes already imposed in the ports.

Appendix

The description of a unit cell as a multiport network and a transfer matrix is particularly helpful when dealing with geometrical symmetries present inside each unit cell. The case of glide and twist symmetries are considered in [19], [55].

A glide-symmetric unit cell is invariant under a mirroring operation and a translation of half a period. In this case, the

eigenproblem can be formulated by means of the transfer matrix of a half cell $[\hat{\mathbf{T}}]$ and a geometric diagonal matrix $[\mathbf{Q}]$:

$$[\hat{\mathbf{T}}] \begin{bmatrix} \mathbf{V} \\ \mathbf{I} \end{bmatrix} = \mathrm{e}^{\gamma p/2} \begin{bmatrix} [\mathbf{Q}] & [\mathbf{0}] \\ [\mathbf{0}] & [\mathbf{Q}] \end{bmatrix} \begin{bmatrix} \mathbf{V} \\ \mathbf{I} \end{bmatrix} . \tag{29}$$

The diagonal entries q_{ii} of $[\mathbf{Q}]$ describe the mirroring of each mode, and are simply $q_{ii} = 1$ if the ith mode is even and $q_{ii} = -1$ if the i-th mode is odd with respect to the mirroring direction. It should be noted that in a 2-D glide-symmetric case, the reduced unit cell is one quarter of a *non-minimal* unit cell, obtained by a suitable rotation of the minimal one [19].

A twist-symmetric cell is invariant under a rotation of $2\pi/n$ and a translation of a period divided by n, with n being an integer. In this case, the problem can still be formulated as in (29), with $[\hat{\mathbf{T}}]$ now being the transfer matrix of one n-th of the period and $\mathrm{e}^{\gamma p/n}$ substituting $\mathrm{e}^{\gamma p/2}$.

Two equivalent choices are possible for the azimuthal dependence of the port modes: one can adopt either a basis of imaginary exponentials or of trigonometric functions. Let us assume that the i-th mode at the ports of the unit cell has an imaginary *exponential* azimuthal variation $\mathrm{e}^{\mathrm{j}n_i\varphi}$, with n_i being a suitable integer. In this case, the $[\mathbf{Q}]$ matrix is a diagonal matrix whose diagonal elements describe the rotation of each mode, and are simply given by $q_{ii} = \mathrm{e}^{\mathrm{j}n_i 2\pi/n}$.

If the i-th mode has a *sinusoidal* azimuthal variation of the kind $\cos(n_i\varphi)$ or $\sin(n_i\varphi)$, the $[\mathbf{Q}]$ matrix is a block diagonal matrix, whose blocks are defined as

$$[\mathbf{Q}_{ii}] = \begin{bmatrix} \cos\left(n_i \dfrac{2\pi}{n}\right) & \sin\left(n_i \dfrac{2\pi}{n}\right) \\ -\sin\left(n_i \dfrac{2\pi}{n}\right) & \cos\left(n_i \dfrac{2\pi}{n}\right) \end{bmatrix} . \tag{30}$$

REFERENCES

[1] N. W. Ashcroft and N. D. Mermin, *Solid State Physics*. Orlando: Harcourt, 1976.

[2] R. E. Collin, *Field Theory of Guided Waves*, 2nd ed. New York: IEEE Press, 1990.

[3] K. Kurokawa, *An Introduction to the Theory of Microwave Circuits*. New Jersey: Academic Press, 1969.

[4] F. Xu, K. Wu, and W. Hong, "Equivalent resonant cavity model of arbitrary periodic guided-wave structures and its application to finite-difference frequency-domain algorithm," *IEEE Trans. Microw. Theory Techn.*, vol. 55, no. 4, pp. 697–702, 2007.

[5] D. G. Dudley, *Mathematical Foundations for Electromagnetic Theory*. New York: Wiley–IEEE Press, 1994.

[6] A. Ishimaru, *Electromagnetic Wave Propagation, Radiation, and Scattering*. New Jersey: Prentice Hall, 1991.

[7] T. Rozzi, L. Pierantoni, and M. Farina, "Eigenvalue approach to the efficient determination of the hybrid and complex spectrum of inhomogeneous, closed waveguide," *IEEE Trans. Microw. Theory Techn.*, vol. 45, no. 3, pp. 345–353, 1997.

[8] M. J. Freire, F. Mesa, and M. Horno, "Excitation of complex and backward mode on shielded lossless printed lines," *IEEE Trans. Microw. Theory Techn.*, vol. 47, no. 7, pp. 1098–1105, 1999.

[9] T. Tamir and A. Oliner, "Guided Complex Waves. Part I. Fields at an interface," *Proc. IEE*, vol. 110, no. 2, pp. 310–334, 1963.

[10] F. Mesa, D. Jackson, and M. Freire, "High frequency leaky-mode excitation on a microstrip line," *IEEE Trans. Microw. Theory Techn.*, vol. 49, no. 12, pp. 2206–2215, 2001.

[11] M. Tsuji, S. Matsumoto, H. Shigesawa, and K. Takiyama, "Guided-Wave Experiments with Dielectric Waveguides Having Finite Periodic Corrugation," *IEEE Trans. Microw. Theory Techn.*, vol. 31, no. 4, pp. 337–344, 1983.

[12] H. K. Liu and T. L. Dong, "Propagation characteristics for periodic waveguide based on generalized conservation of complex power technique," *IEEE Trans. Microw. Theory Techn.*, vol. 54, no. 9, pp. 3479–3485, 2006.

[13] B. Bandlow, R. Schuhmann, G. Lubkowski, and T. Weiland, "Analysis of single-cell modeling of periodic metamaterial structures," *IEEE Trans. Magnet.*, vol. 44, no. 6, pp. 1662–1665, 2008.

[14] Y. Weitsch and T. F. Eibert, "Periodically loaded waveguide analysis by propagating and evanescent mode superposition," in *Proc. of the European Microwave Conference, EuMC 2009.*, Oct. 2009, pp. 1271–1274.

[15] F. Bongard, J. Perruisseau-Carrier, and J. R. Mosig, "Enhanced periodic structure analysis based on a multiconductor transmission line model and application to metamaterials," *IEEE Trans. Microw. Theory Techn.*, vol. 57, no. 11, pp. 2715–2726, 2009.

[16] R. Islam, M. Zedler, and G. V. Eleftheriades, "Modal analysis and wave propagation in finite 2D transmission-line metamaterials," *IEEE Trans. Antennas Propag.*, vol. 59, no. 5, pp. 1562–1570, 2011.

[17] J. Naqui, A. Fernández-Prieto, M. Durán-Sindreu, F. Mesa, J. J. Martel, F. Medina, and F. Martín, "Common-mode suppression in microstrip differential lines by means of complementary split ring resonators: Theory and applications," *IEEE Trans. Microw. Theory Techn.*, vol. 60, no. 10, pp. 3023–3034, 2012.

[18] Y. Weitsch and T. F. Eibert, "Modal series expansion of eigensolutions for closed and open periodic waveguides," *IEEE Trans. Antennas Propag.*, vol. 60, no. 12, pp. 5881–5889, 2012.

[19] M. Bagheriasl, O. Quevedo-Teruel, and G. Valerio, "Bloch analysis of artificial lines and surfaces exhibiting glide symmetry," *IEEE Trans. Microw. Theory Techn.*, vol. 67, no. 7, pp. 2618–2628, 2019.

[20] A. F. Peterson, S. L. Ray, and R. Mittra, *Computational Methods for Electromagnetics*. New York: Wiley–IEEE Press, 1997.

[21] R. F. Harrington, *Field Computation by Moment Methods*. New York: Wiley–IEEE Press, 1993.

[22] J.-M. Jin, *The Finite Element Method in Electromagnetics*, 3rd ed. New York: Wiley–IEEE Press, 2014.

[23] R.-B. Hwang, *Periodic Structures: Mode-Matching Approach and Applications in Electromagnetic Engineering*. New York: Wiley–IEEE Press, 2012.

[24] M. S. Tong and W. C. Chew, *The Nystrom Method in Electromagnetics*. New York: Wiley–IEEE Press, 2019.

[25] D. M. Pozar, *Microwave Engineering*, 4th ed. New York: John Wiley, 1990.

[26] G. Conciauro, M. Bressan, and C. Zuffada, "Waveguide modes via an integral equation leading to a linear matrix eigenvalue problem," *IEEE Trans. Microw. Theory Techn.*, vol. 32, no. 11, pp. 1495–1504, 1984.

[27] P. Lampariello and R. Sorrentino, "The ZEPLS program for solving characteristic equations of electromagnetic structures (computer program descriptions)," *IEEE Trans. Microw. Theory Techn.*, vol. 23, no. 5, pp. 457–458, 1975.

[28] M. A. Marin, S. Barkeshli, and P. H. Pathat, "On the location of proper and improper surface wave poles for the grounded dielectric slab," *IEEE Trans. Antennas Propag.*, vol. 38, no. 4, pp. 1317–1324, 1990.

[29] R. Rodríguez-Berral, F. Mesa, and F. Medina, "Appropriate formulation of the characteristic equation for open nonreciprocal layered waveguides with different upper and lower half-spaces," *IEEE Trans. Microw. Theory Techn.*, 2005.

[30] P. Kowalczyk, "Global complex roots and poles finding algorithm based on phase analysis for propagation and radiation problems," *IEEE Trans. Antennas Propag.*, vol. 66, no. 12, pp. 7198–7205, dec 2018.

[31] G. P. Zouros, "CCOMP: An efficient algorithm for complex roots computation of determinantal equations," *Comput. Phys. Commun.*, vol. 222, pp. 339–350, 2018.

[32] P. Baccarelli, C. D. Nallo, S. Paulotto, and D. R. Jackson, "A full-wave numerical approach for modal analysis of 1-D periodic microstrip structures," *IEEE Trans. Microw. Theory Techn.*, vol. 54, no. 4, pp. 1350–1362, 2006.

[33] P. Harms, R. Mittra, and W. Ko, "Implementation of the periodic boundary condition in the finite-difference time-domain algorithm for FSS structures," *IEEE Trans. Antennas Propag.*, vol. 42, no. 9, pp. 1317–1324, 1994.

[34] M. Celuch-Marcysiak and W. K. Gwarek, "Spatially Looped Algorithms for Time-Domain Analysis of Periodic Structures," *IEEE Trans. Microw. Theory Techn.*, vol. 43, no. 4, pp. 860–865, 1995.

[35] M. Chen, B. Houshmand, and T. Itoh, "FDTD analysis of a metal-strip-loaded dielectric leaky-wave antenna," *IEEE Trans. Antennas Propag.*, vol. 45, no. 8, pp. 1294–1301, 1997.

[36] T. Kokkinos, C. D. Sarris, and G. V. Eleftheriades, "Periodic FDTD analysis of leaky-wave structures and applications to the analysis of negative-refractive-index leaky-wave antennas," *IEEE Trans. Microw. Theory Techn.*, vol. 54, no. 4, pp. 1619–1630, 2006.

[37] N. Marcuvitz, *Waveguide Handbook*. New York: McGraw-Hill, 1951.

[38] G. Valerio, Z. Sipus, A. Grbic, and O. Quevedo-Teruel, "Accurate equivalent-circuit descriptions of thin glide-symmetric corrugated metasurfaces," *IEEE Trans. Antennas Propag.*, vol. 65, no. 5, pp. 2695–2700, may 2017.

[39] S. Amari, R. Vahldieck, J. Bornemann, C. Forces, and C. Angel, "Accurate analysis of periodic structures with an additional symmetry in the unit cell from classical matrix eigenvalues," *IEEE Trans. Microw. Theory Techn.*, vol. 46, no. 10, pp. 1513–1515, 1998.

[40] F. Mesa, R. Rodríguez-Berral, and F. Medina, "On the computation of the dispersion diagram of symmetric one-dimensionally periodic structures," *Symmetry (Basel).*, vol. 10, no. 8, p. 307, 2018.

[41] M. Bozzi, S. Germani, L. Minelli, L. Perregrini, and P. de Maagt, "Efficient calculation of the dispersion diagram of planar electromagnetic band-gap structures by the MoM/BI-RME method," *IEEE Trans. Antennas Propag.*, vol. 53, no. 1, pp. 29–35, 2005.

[42] J. E. Varela and J. Esteban, "Analysis of laterally open periodic waveguides by means of a generalized transverse resonance approach," *IEEE Trans. Microw. Theory Techn.*, vol. 59, no. 4 PART 1, pp. 816–826, 2011.

[43] M. Kahrizi, T. K. Sarkar, and Z. A. Maricevic, "Dynamic analysis of a microstrip line over a perforated ground plane," *IEEE Trans. Microw. Theory Techn.*, vol. 42, no. 5, pp. 820–825, 1994.

[44] L. Zhu, "Guided-wave characteristics of periodic coplanar waveguides with inductive loading-unit-length transmission parameters," *IEEE Trans. Microw. Theory Techn.*, vol. 51, no. 10, pp. 2133–2138, 2003.

[45] Y. C. Chen, C. K. C. Tzuang, T. Itoh, and T. K. Sarkar, "Modal characteristics of planar transmission lines with periodical perturbations: Their behaviors in bound, stopband, and radiation regions," *IEEE Trans. Antennas Propag.*, vol. 53, no. 1, pp. 47–58, 2005.

[46] M. Bozzi, M. Pasian, L. Perregrini, and K. Wu, "On the losses in substrate-integrated waveguides and cavities," *Int. J. Microw. Wirel. Technol.*, vol. 1, no. 5, pp. 395–401, 2009.

[47] G. Valerio, S. Paulotto, P. Baccarelli, P. Burghignoli, and A. Galli, "Accurate Bloch analysis of 1-D periodic lines through the simulation of truncated structures," *IEEE Trans. Antennas Propag.*, vol. 59, no. 6, pp. 2188–2195, 2011.

[48] A. Morini and T. Rozzi, "On the generalized scattering matrix of a lossless multiport," *IEEE Trans. Microw. Theory Techn.*, vol. 49, no. 1, pp. 160–165, 2001.

[49] J. A. Dobrowlski, *Microwave Network Design Using the Scattering Matrix*. Englewood Cliffs (New Jersey): Artech House, 2010.

[50] J. Frei, X.-D. Cai, and S. Muller, "Multiport S-Parameter and T-Parameter Conversion With Symmetry Extension," *IEEE Trans. Microw. Theory Techn.*, vol. 56, no. 11, pp. 2493–2504, 2008.

[51] J. Shekel, "Matrix Analysis of Multi-Terminal Transducers," *Proc. IRE*, vol. 42, no. 5, pp. 840–847, 1954.

[52] T. Reveyrand, "Multiport conversions between S , Z , Y , h , ABCD , and T parameters," in *2018 Int. Work. Integr. Nonlinear Microw. Millimetre-wave Circuits*, no. 6, 2018, pp. 1–3.

[53] A. Hessel, , M. H. Chen, R. C. Li, and A. A. Oliner, "Propagation in Periodically Loaded Waveguides with Higher Symmetries," *Proc. IEEE*, vol. 61, no. 2, pp. 183–195, 1973.

[54] F. Ghasemifard, M. Norgren, and O. Quevedo-Teruel, "Twist and polar glide symmetries: an additional degree of freedom to control the propagation characteristics of periodic structures," *Scientific Reports*, vol. 8, no. 11266, July 2018.

[55] M. Bagheriasl and G. Valerio, "Bloch analysis of electromagnetic waves in twist-symmetric lines," *Symmetry (Basel).*, vol. 11, no. 5, pp. 1–11, 2019.

[56] G. Valerio, S. Paulotto, P. Baccarelli, D. R. Jackson, D. R. Wilton, W. A. Johnson, and A. Galli, "Efficient computation of 1-D periodic layered mixed potentials for the analysis of leaky-wave antennas with vertical elements," *IEEE Trans. Antennas Propag.*, vol. 63, no. 6, pp. 2396–2411, 2015.

[57] L. Wang, J. L. Gomez-Tornero, E. Rajo-Iglesias, and O. Quevedo-Teruel, "Low-dispersive leaky-wave antenna Integrated in groove gap waveguide technology," *IEEE Trans. Antennas Propag.*, vol. 66, no. 11, pp. 5727–5736, 2018.

[58] M. Vukomanovic, J. Vazquez-Roy, O. Quevedo-Teruel, E. Rajo-Iglesias, and Z. Sipus, "Gap waveguide leaky-wave antenna," *IEEE Trans. Antennas Propag.*, vol. 64, no. 5, pp. 2055–2060, May 2016.

[59] M. Ebrahimpouri, E. Rajo-Iglesias, Z. Sipus, and O. Quevedo-Teruel, "Cost-effective gap waveguide technology based on glide-symmetric holey EBG structures," *IEEE Trans. Microw. Theory Techn.*, vol. 66, no. 2, pp. 927–934, Feb 2018.

[60] O. Quevedo-Teruel, J. Miao, M. Mattsson, A. Algaba-Brazalez, M. Johansson, and L. Manholm, "Glide-symmetric fully metallic Luneburg lens for 5G communications at Ka-band," *IEEE Antennas Wirel. Propag. Lett.*, vol. 17, no. 9, pp. 1588–1592, Sept 2018.